2023 62nd IEEE Conference on Decision and Control (CDC)
December 13-15, 2023. Marina Bay Sands, Singapore

Quasi-Static Mechanical Manipulation as an Optimal Process

Domenico Campolo[1] and Franco Cardin[2]

***Abstract*— This work focuses on *quasi-static manipulation* of elastically-interconnected rigid bodies by an agent, e.g. a robot assembling mechanical parts. The whole system is seen as an underactuated control problem, where only certain degrees of freedom (e.g. robot end-effector) are directly controllable. Mechanical contact is regularized via nonlinear yet smooth elastic interaction giving rise to a smooth total potential energy. The squared-Hessian of such a potential is used as optimality measure and quasi-static mechanical manipulation is rephrased as optimal path planning on the manifold of mechanical equilibria. A simple example of an elastically-driven inverted pendulum is presented as a toy model. Numerical implementation as a minimum path on graphs is also described.**

I. Introduction

This work focuses on *quasi-static manipulation* of elastically-interconnected rigid bodies and proposes an *optimality* measure based on a *squared-Hessian*, derived from the mechanical potential energy of the system.

From an applied robotics perspective, since the early work of Whitney [23], it has been clear that quasi-static frameworks are central to the analysis of many tasks related to robotic assembly and manipulation [18], [19], [14], [22], [15], [24]. From a more theoretical perspective, a suitable geometric framework whereby not only kinematic configurations but also interaction forces can be represented, was brought to the attention of the robotics community by Brockett and Stokes [3]. These more geometrical aspects are emphasized in an extended version of this work [6], while here the analysis will be confined to the kinematic configuration space. The purpose of this work is to emphasize the role of *stiffness as a metric* for the purpose of mechanical manipulation. In fact, since the 90's, Loncaric [16], [17] already indicated *stiffness* as a possible source of positive-definite matrices, in addition to inertia and damping. Elastic interactions can be captured via (scalar) elastic potentials and in particular their *Hessian*, or stiffness matrix, at critical points (the only points where Hessians behave tensorially) [17].

A discipline that offers insights on the use of stiffness as a metric for quasi-static processes is *thermodynamics*. Classical thermodynamics studies processes at equilibrium, the reader is also referred to the recent review by van der Schaft [21]. The Hessian of thermodynamic potentials (e.g. internal entropy) are positive-definite (by the second principle of thermodynamics) and have been used to define a possible metric, see [8] and reference therein.

Inspired by these works, we propose describing a *'quasi-static' mechanical manipulation as an optimal control problem*. Assuming a quasi-static evolution, as the control variables are slowly varied, the internal variables undergo changes along the so-called *equilibrium manifold*. The main novelty of this work is that *optimality* will be based on an ad-hoc metric derived from the *squared-Hessian of the elastic potential*. However, unlike the thermodynamic approach [8], where the Hessian itself enjoys positive-definiteness, we will resort to a squared-Hessian (non-negative by definition). For more details and justifications of this choice, the reader is referred to [6].

Finally, once the problem is stated as a quasi-static optimal process, one is faced with the *computational complexity* inherent with the derivation of numerical solutions. To partially address this problem, we show how to 'rephrase' the quasi-static manipulation problem as an optimal path planning problem on the equilibrium manifold. This allows to readily re-adapt various algorithms originally developed for robotic motion planning [12], many of which are graph based [25]. To illustrate all the steps above, a toy model of an elastically-driven pendulum is presented. Equilibria are numerically derived and captured as vertices of a graph. Connections and weights of the graph are defined via the squared-Hessian optimality measure and the minimum path.

Unlike classical robot navigation problems, an interesting aspect arising in mechanical manipulation problems, which is inherent to elastic stability, is the possible *multivaluedness* of equilibria. To this end, an algorithm is sketched which defines the connectivity of a graph based on the first order approximation of the equilibrium manifold, i.e. it allows identifying the 'true' neighbor despite a multiplicity of equilibria.

II. Interconnected mechanical systems

Following [5], the configuration space Q of interconnected mechanical systems can be thought of as a C^∞-immersed submanifold of the product space

$$Q \subset \underbrace{SE(3) \times \cdots \times SE(3)}_{N_b \text{ rigid bodies}} \times \underbrace{\mathbb{R}^3 \times \cdots \times \mathbb{R}^3}_{N_p \text{ particles}} \qquad (1)$$

of dimension $\dim Q \leq 6N_b + 3N_p$. We shall assume that $K \geq 1$ degrees of freedom (dof) are directly controllable by an agent while the remaining $N = \dim Q - K$ dof can only be indirectly influenced via generalized elastic forces or via external forces such as gravity. In robotics, such systems are often referred to as '*underactuated*', meaning that the

[1]Domenico Campolo is with the School of Mechanical and Aerospace Engineering, Nanyang Technological University (NTU), Singapore. d.campolo@ntu.edu.sg

[2]Franco Cardin is with the Dipartimento di Matematica "Tullio Levi-Civita", Università degli Studi di Padova, Italy. cardin@math.unipd.it

directly controllable dof (K) is strictly less than the total number of dof ($\dim Q$).

The analysis that follows is mostly local, relying on the Implicit Function theorem and on Taylor's expansion as main analytical tools. In particular, we shall assume the existence of equilibria in some open neighborhood of Q parameterized via a set of coordinates $(\boldsymbol{z}, \boldsymbol{u}) \in \mathcal{Z} \times \mathcal{U}$, where $\mathcal{Z} \subset \mathbb{R}^N$ and $\mathcal{U} \subset \mathbb{R}^K$ are open sets. These coordinates represent

- **internal states** $\boldsymbol{z} \in \mathcal{Z} \subset \mathbb{R}^N$, non directly controllable (i.e. under-actuated)
- **control inputs** $\boldsymbol{u} \in \mathcal{U} \subset \mathbb{R}^K$, directly controllable by the agent, therefore assumed as an input to the system.

We shall further assume that the system will solely be subjected to conservative forces (either via gravity or internal springs) and, in particular, the existence of a smooth (C^∞) potential energy

$$W(\boldsymbol{z}, \boldsymbol{u}) : \mathcal{Z} \times \mathcal{U} \to \mathbb{R} \tag{2}$$

Considering the control inputs $\boldsymbol{u}$ as parameters, mechanical equilibria correspond to stationary points of the potential with respect to internal variables $\boldsymbol{z}$, which is equivalent to a zero-condition for internal forces[1] $\nabla_{\boldsymbol{z}} W$. More specifically, for a given control input $\boldsymbol{u}^*$, there exist possibly multiple solutions $\boldsymbol{z}^*_m$ (with $m \geq 1$ being an integer denoting the *multiplicity* of equilibria) to the **equilibrium equation**:

$$\nabla_{\boldsymbol{z}} W(\boldsymbol{z}^*_m, \boldsymbol{u}^*) = \boldsymbol{0} \tag{3}$$

where $\nabla_{\boldsymbol{z}}$ denotes the column[2] operator $[\partial_{z_1} \ \dots \ \partial_{z_N}]^T$ and, similarly, $\nabla_{\boldsymbol{u}} \equiv [\partial_{u_1} \ \dots \ \partial_{u_K}]^T$. We shall further introduce the shorthand notation $\nabla^2_{\boldsymbol{zz}} \equiv \nabla_{\boldsymbol{z}} \nabla^T_{\boldsymbol{z}}$ for the Hessian as well as for the mixed-derivatives operators $\nabla^2_{\boldsymbol{uz}} \equiv \nabla_{\boldsymbol{u}} \nabla^T_{\boldsymbol{z}}$ and $\nabla^2_{\boldsymbol{zu}} \equiv \nabla_{\boldsymbol{z}} \nabla^T_{\boldsymbol{u}} = (\nabla^2_{\boldsymbol{uz}})^T$.

Once the input $\boldsymbol{u}^*$ is fixed, stability of the mechanical system is determined by the positive-definiteness of the Hessian $\nabla^2_{\boldsymbol{zz}} W$ [2]. If the Hessian is full-ranked at a given equilibrium, i.e.

$$\text{rank}(\nabla^2_{\boldsymbol{zz}} W|_{(\boldsymbol{z}^*_m, \boldsymbol{u}^*)}) = N \qquad \textit{(max-rank)} \tag{4}$$

then such an equilibrium will be referred to as *non-critical*.

Assuming the existence of one solution and max-rank condition (4), then by the Implicit Function Theorem, here restated as in [20, Th. 2-12], there exist an open $\mathcal{U}' \subset \mathcal{U}$ containing $\boldsymbol{u}^*$, an open set $\mathcal{Z}' \subset \mathcal{Z}$ containing $\boldsymbol{z}^*$ and a differentiable map $\boldsymbol{z}_m : \mathcal{U}' \to \mathcal{Z}'$ such that $\boldsymbol{z}_m(\boldsymbol{u}) \in \mathcal{Z}'$ is *unique* and $\nabla_{\boldsymbol{z}} W(\boldsymbol{z}_m(\boldsymbol{u}), \boldsymbol{u}) = \boldsymbol{0}$, for all $\boldsymbol{u} \in \mathcal{U}'$.

The **Equilibrium Manifold** (EM) can be described as a K-dimensional submanifold

$$\text{EM} = \{(\boldsymbol{z}, \boldsymbol{u}) \in \mathbb{R}^N \times \mathbb{R}^K \ : \ \nabla_{\boldsymbol{z}} W(\boldsymbol{z}, \boldsymbol{u}) = \boldsymbol{0}\} \tag{5}$$

which can be parameterized by controls $\boldsymbol{u}$, at least locally, in an open neighborhood of a non-critical equilibrium $\boldsymbol{z}^*_m, \boldsymbol{u}^*$.

In summary, for a given control input $\boldsymbol{u}^*$, the equilibrium equation (3) can be solved (e.g. numerically) to derive possibly multiple solutions $(\boldsymbol{z}^*_m, \boldsymbol{u}^*)$, with multiplicity index $m = 1, 2, \dots$. Around each solution $(\boldsymbol{z}^*_m, \boldsymbol{u}^*)$ satisfying[3] the max-rank condition (4), there exists an open neighborhood $\mathcal{Z}' \times \mathcal{U}'$ on which the EM is a submanifold and we shall refer to it as *local branch* of EM.

III. Gilmore's metric on the EM

The derivation below mostly follows [8, §5] but with some difference which will be highlighted. The final objective is to approximate (by 2nd order Taylor expansion) the potential $W_m(\boldsymbol{u}) = W(\boldsymbol{z}_m(\boldsymbol{u}), \boldsymbol{u})$ around the equilibrium $(\boldsymbol{z}^*_m, \boldsymbol{u}^*)$.

1) First order analysis: Consider curves on the EM

$$s \mapsto (\boldsymbol{z}_m(\boldsymbol{u}(s)), \boldsymbol{u}(s)) \in \text{EM}$$

parameterized by a scalar $s \in \mathbb{R}$, at least locally, such that which $\boldsymbol{u}(0) = \boldsymbol{u}^*$ and $\boldsymbol{z}_m(\boldsymbol{u}(0)) = \boldsymbol{z}^*_m$. For every such curve, the equilibrium condition (3) is satisfied for all s, i.e.

$$\nabla_{\boldsymbol{z}} W(\boldsymbol{z}_m(\boldsymbol{u}(s)), \boldsymbol{u}^*(s)) = \boldsymbol{0}$$

which, differentiated with respect to s, leads to $\nabla^2_{\boldsymbol{zz}} W \nabla_{\boldsymbol{u}} \boldsymbol{z}_m \dot{\boldsymbol{u}} + \nabla^2_{\boldsymbol{uz}} W \dot{\boldsymbol{u}} = \boldsymbol{0}$ or

$$\nabla_{\boldsymbol{u}} \boldsymbol{z}_m \dot{\boldsymbol{u}} = -(\nabla^2_{\boldsymbol{zz}} W)^{-1} \nabla^2_{\boldsymbol{uz}} W \dot{\boldsymbol{u}}$$

where $\dot{\boldsymbol{u}} = d\boldsymbol{u}/ds$. Rewriting in terms of differentials $\delta \boldsymbol{u} := \dot{\boldsymbol{u}} ds$ and $\delta \boldsymbol{z} := \nabla_{\boldsymbol{u}} \boldsymbol{z}_m \delta \boldsymbol{u}$, to maintain similarity with the nomenclature in [8, §5], leads to the condition

$$\boxed{\delta \boldsymbol{z} = -(\nabla^2_{\boldsymbol{zz}} W)^{-1} \nabla^2_{\boldsymbol{uz}} W \delta \boldsymbol{u}} \tag{6}$$

2) Second order analysis: Expanding up to the second order the potential $W(\boldsymbol{z}_m(\boldsymbol{u}), \boldsymbol{u})$ around an equilibrium $(\boldsymbol{z}^*_m, \boldsymbol{u}^*)$, denoted as $|_*$ for short, leads [4] to

$$W(\boldsymbol{z}^* + \delta \boldsymbol{z}, \boldsymbol{u}^* + \delta \boldsymbol{u}) = W(\boldsymbol{z}^*_m, \boldsymbol{u}^*) + \delta \boldsymbol{u}^T \boldsymbol{f}^{eq}_m + \\ + \tfrac{1}{2} \delta \boldsymbol{u}^T \boldsymbol{G}_m(\boldsymbol{u}) \, \delta \boldsymbol{u} + \mathcal{O}(3)$$

where $\boldsymbol{f}^{eq}_m$ is the (static) control force required to maintain equilibrium, defined as

$$\boxed{\boldsymbol{f}^{eq}_m(\boldsymbol{u}) := -\nabla_{\boldsymbol{u}} W} \tag{7}$$

while the $K \times K$ *control Hessian* $\boldsymbol{G}_m(\boldsymbol{u})$ is defined as

$$\boxed{\boldsymbol{G}_m(\boldsymbol{u}) := \nabla^2_{\boldsymbol{uu}} W - \nabla^2_{\boldsymbol{zu}} W (\nabla^2_{\boldsymbol{zz}} W)^{-1} \nabla^2_{\boldsymbol{uz}} W} \tag{8}$$

where all derivatives are evaluated at a given equilibrium $(\boldsymbol{z}_m(\boldsymbol{u}^*), \boldsymbol{u}^*)$.

Remark: In general[5], we cannot assume positive-definiteness of the control Hessian (8), as also evident by

[1] With perhaps an abuse of notation, the wording "internal forces" really refers to gradients with respect to "internal" variables $\boldsymbol{z}$, this also includes gravity which is definitely not internal to the system.

[2] In this work, both vectors $\delta \boldsymbol{z} = [\delta z_1, \dots, \delta z_N]^T$ and covectors $\nabla_{\boldsymbol{z}} W = [\partial_{z_1} W \ \dots \ \partial_{z_2} W]^T$ will be represented as a column arrays. The natural pairing $\langle \nabla_{\boldsymbol{z}} W, \delta \boldsymbol{z} \rangle$ will then be evaluated in matrix notation as $(\nabla_{\boldsymbol{z}} W)^T \delta \boldsymbol{z} = \nabla^T_{\boldsymbol{z}} W \delta \boldsymbol{z}$.

[3] Satisfying max-rank condition (4) is equivalent to verifying $\det(\nabla^2_{\boldsymbol{zz}} W|_*) \neq 0$.

[4] The derivation is omitted for brevity but can be found in [8, eq.(5.1)-(5.3)], albeit with different notation.

[5] In [8, §10.12], Gilmore applies the same definition to a thermodynamic problem where, due to the special interrelations of thermodynamic variables, (8) can be assumed positive definite.

the simple example described in the next section. For this reason, we propose the use of the **squared-Hessian** $\boldsymbol{G}_m^2(\boldsymbol{u})$ as possible metric to define optimal paths on the equilibrium manifold.

IV. Toy Example: Manipulation of an Elastically-Driven Inverted Pendulum

In this section, the theory developed earlier will be applied to a simple 2D pendulum elastically driven by an agent. With reference to Fig. 1, we consider the task of stabilizing an inverted pendulum in its upward position, in the space frame $\{0\}$. The pendulum consists of a rigid body $\mathcal{B} \subset \mathbb{E}^2$ (i.e. $\mathbb{R}^2$ with the usual Euclidean distance). For simplicity, we shall assume a uniform, rectangular bar of length L_0 with center of mass (com) located at its geometric center.

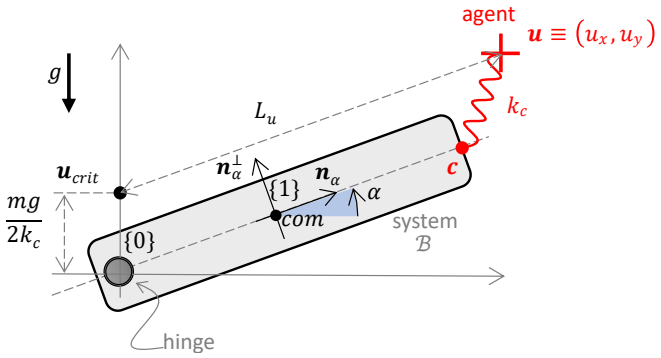

Fig. 1. Inverted Pendulum

We shall consider a moving-frame $\{1\}$ attached to the com of the pendulum and rotating with it by angle α (see Fig.1) with respect to the space-frame frame $\{0\}$. For convenience, we shall define the (unit-length) axis $\boldsymbol{n}_\alpha$ directed along the major axis, the (unit-length) axis $\boldsymbol{n}_\alpha^\perp$ perpendicular to it as well as the rotation matrix $\boldsymbol{R}_\alpha$ as follows:

$$\boldsymbol{n}_\alpha = \begin{bmatrix}\cos\alpha \\ \sin\alpha\end{bmatrix} \quad \boldsymbol{n}_\alpha^\perp = \begin{bmatrix}-\sin\alpha \\ \cos\alpha\end{bmatrix} \quad \boldsymbol{R}_\alpha = \begin{bmatrix}\cos\alpha & -\sin\alpha \\ \sin\alpha & \cos\alpha\end{bmatrix}$$

As shown in Fig.1, the pendulum is subject to a gravitational potential W_{grav} (due to a constant force mg, pointing downwards and acting at com) as well as to the elastic (control) potential W_{ctrl} due to a *nonlinear* spring of stiffness k_c attached between an agent-controlled position $\boldsymbol{u} = (u_x, u_y)$ and the tip of the pendulum $\boldsymbol{c} = L_0\boldsymbol{n}_\alpha$. The total potential W can then be expressed as

$$\begin{aligned} W(\alpha, \boldsymbol{u}) &= W_{grav} + W_{ctrl} \\ &= \tfrac{1}{2}mgL_0\sin\alpha + \tfrac{1}{2}k_c\|\boldsymbol{u} - L_0\boldsymbol{n}_\alpha\|^2 \\ &= \tfrac{1}{2}mgL_0\sin\alpha + \tfrac{1}{2}k_c((u_x - L_0\cos\alpha)^2 \\ &\quad +(u_y - L_0\sin\alpha)^2) \end{aligned} \tag{9}$$

In the case of a linear spring k_c, the control Hessian (8) can be derived by differentiating (9) resulting in the following expression (detailed calculations are reported in [6]):

$$\boldsymbol{G}_m(\boldsymbol{u}) = \boldsymbol{R}_{\alpha^*}\begin{bmatrix}k_c & 0 \\ 0 & k_c\left(1 - \frac{L_0}{L_u}\right)\end{bmatrix}\boldsymbol{R}_{\alpha^*}^T \tag{10}$$

where α^* is the **stable equilibrium**

$$\alpha^* := \boldsymbol{z}_0^*(\boldsymbol{u}) = \text{atan2}(u_y - mg/2k_c, u_x) \tag{11}$$

and L_u is the control length, defined as

$$L_u := \|\boldsymbol{u} - \boldsymbol{u}_{crit}\| = \sqrt{u_x^2 + (u_y - mg/2k_c)^2} \tag{12}$$

and $\boldsymbol{u}_{crit} := u_y - mg/2k_c$ is the control input for which $L_u = 0$, rendering the control Hessian ill-defined.

Remark: By simple inspection of (10), it is evident that the one of the eigenvalues of $\boldsymbol{G}_m(\boldsymbol{u})$ is negative if $L_u < L_0$ and positive if $L_u > L_0$.

For this reason, we propose to consider the **squared-Hessian** $\boldsymbol{G}_m^2$ as a possible metric[6] and formulate the quasi-static manipulation problems as an optimal problem via minimization of the action

$$J = \int_{\alpha_1}^{\alpha_2} \boldsymbol{u}'^T \boldsymbol{G}_m^2 \boldsymbol{u}'\, d\alpha \tag{13}$$

A. Regularized mechanical contact via nonlinear compliance

One of major hurdles in robotic manipulation is the non-smooth nature of mechanical contact [4] for which there exist various possible approaches. Here we would like to be able to make use of the optimal control framework derived so far, for which smoothness is essential. We therefore propose to *regularize* contact between two bodies (e.g. $\mathcal{B}_1$ and $\mathcal{B}_2$) via a non-linear stiffness k_c which depends on the *inter-penetration* d, as sketched in Fig. 2.

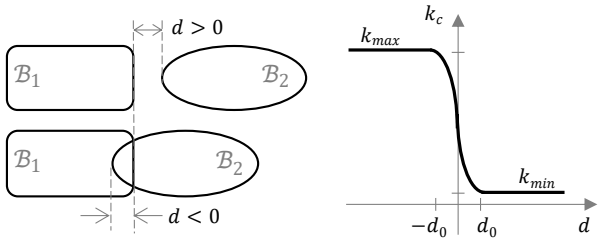

Fig. 2. Regularization of mechanical contact: based on the penetration variable d, a spring of with nonlinear stiffness k_c is designed assuming high-stiffness levels (k_{max}) when the bodies are in contact ($d < 0$) and low-stiffness levels (k_{min}) when not in contact $d > 0$. A steep yet smooth transition occurs in an interval $[-d_0\ d_0]$.

Inter-penetration is a *signed distance*: if two objects are in mechanical contact, we allow for some degree of inter-penetration ($d < 0$) and high contact forces arise from the assumption of a high level of stiffness (k_{max}). On the other hand, when the two objects are not in contact ($d > 0$), one would expect no forces and this is modeled via a very low[7] level of stiffness ($k_{min} \ll k_{max}$). We then assume a steep yet smooth transition (around $d \approx 0$) as sketched in the

[6]It can be shown that both $\boldsymbol{G}_m$ and $\boldsymbol{G}_m^2$ behave tensorially with respect to change of coordinates.

[7]A very low but non-zero stiffness is *essential* as it provides useful non-zero gradients for the (virtual) agent to find a path even when not in contact. It turns out to be a very useful expedient to make robotic agents aware of their surroundings. For example, in [10], virtual 'proxies' are introduced to guide the robot towards the goal before any contact is even made.

graph in Fig. 2. Analytically, this can be modeled via smooth functions such as

$$k_c(d) = k_{min} + \frac{1 - \tanh(d/d_0)}{2} k_{max} \tag{14}$$

where d_0 is a parameter capturing the penetration depth.

Computing the inter-penetration of rigid bodies for generic shapes can be computationally expensive and is typically done via numerical methods [11]. The task is much simpler when one of the bodies can be assumed to be a point, as in the case of the agent[8] in Fig.1, represented by a point of coordinates $\boldsymbol{u} = (u_x, u_y)$.

With reference to the specific 2D problem in Fig 1, to compute the penetration d by the agent, localized at given point $\boldsymbol{u}$, within the rigid body of the pendulum, a geometrical definition of the shape of the pendulum is required. Both in 2D as well as in 3D, a simple way to proceed analytically is to model the rigid body $\mathcal{B}$ as a *super-ellipse* [9], for which the pseudo-distance d between agent and body $\mathcal{B}$ is simply given as

$$d := \Delta(u_x, u_y)$$

where $\Delta : \mathbb{E}^2 \to \mathbb{R}$ is the super-ellipse *inside-outside function*

$$\Delta : (x, y) \mapsto \left(\frac{x}{a}\right)^{2/\epsilon} + \left(\frac{y}{b}\right)^{2/\epsilon} - 1 \tag{15}$$

where $0 < \epsilon < 2$ define the shape of the super-ellipse ($\epsilon = 1$ for an ellipse, $\epsilon < 1$ for a super-ellipse as in this work), while a and b represent half-length and half-width of the body $\mathcal{B}$, respectively.

B. Equilibrium Manifold

The configuration space Q of the agent+pendulum can be parameterized by the (scalar) rotation $z \equiv \alpha \in \mathbb{R}$ of the pendulum and the 2D position $\boldsymbol{u} \equiv (u_x, u_y) \in \mathbb{R}^2$ of the agent, resulting in the three-dimensional manifold:

$$Q := S^1 \times \mathbb{R}^2 \tag{16}$$

As our analysis is local, we shall assume working in an open of $\mathbb{R} \times \mathbb{R}^2$.

The total potential W will comprise a gravitational potential W_{grav} and the (control) elastic potential W_{ctrl} and will be formally similar to (9). The only difference is due to the nonlinearity of the stiffness k_c, now function of the inter-penetration d which can readily be evaluated via the super-ellipse function $\Delta(\cdot)$ defined in (15). This valuation is more conveniently done in the moving frame:

$$W_{ctrl} = \frac{1}{2} k_c(\Delta(\tilde{\boldsymbol{u}}))\ \|\tilde{\boldsymbol{u}} - \tilde{\boldsymbol{c}}\|^2 \tag{17}$$

where $\|\cdot\|^2$ is the Euclidean distance; the tilde $\tilde{\cdot}$ denotes coordinates expressed in the moving frame $\{1\}$, in which, $\tilde{\boldsymbol{c}}$ is a constant vector and $\tilde{\boldsymbol{u}} := \boldsymbol{T}_1^{-1} \circ \boldsymbol{u}$.

[8]In robotics, this is not uncommon. In the so-called 'force control mode', robots are programmed to impart actual forces based on virtual springs, such as k_c, virtual points such as $\boldsymbol{u}$ and physical points, such as $\boldsymbol{c}$, whose coordinates can be measured, for example, via vision systems.

Thanks to the smoothness of the functions (14) and (15), gradients $\nabla_{\boldsymbol{z}} W$, $\nabla_{\boldsymbol{u}} W$ as well as the second derivatives $\nabla^2_{\boldsymbol{uz}} W$, $\nabla^2_{\boldsymbol{zu}} W$, and the Hessian $\nabla^2_{\boldsymbol{z}} W$ can be computed analytically in symbolic form, via the MATLAB Symbolic Toolbox or any other Computer Algebra System.

Using the numerical values given in Table I, a numerical solver (`fsolve` in MATLAB) was used to solve the equilibrium equation (3) for an array of inputs u_x and u_y, each spanning across 150% of workspace ($\pm L_0$).

parameter	*value*	*units*	*description*
L_0	1	m	pendulum length
W_0	0.1	m	pendulum width
mg	10	N	weight force
k_{min}	1	N/m	stiffness
k_{max}	10^4	N/m	stiffness
ϵ	0.1	-	super-ellipse factor

TABLE I

VALUES USED IN THE NUMERICAL SIMULATIONS.

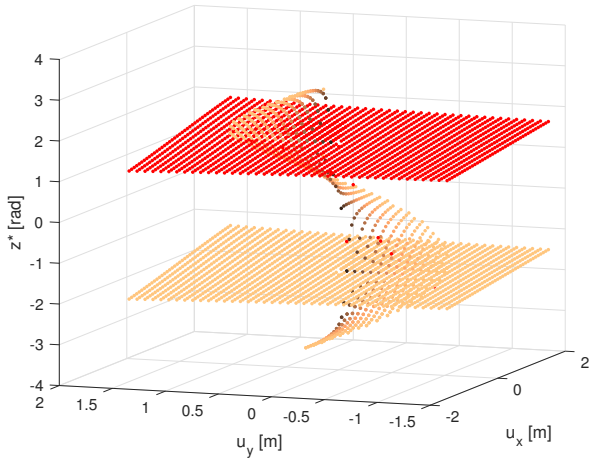

Fig. 3. Equilibrium configurations z^* (equivalent to the rotation α of the pendulum) for an array of inputs (u_x, u_y) spanning 150% of the workspace ($\pm L_0$)

At each point (u_x, u_y) of the grid, multiple solutions z^*_m (a scalar, representing an equilibrium angle α of the pendulum angle), each with its own multiplicity index m, are estimated by the numerical solver and are shown in Fig. 3, where the unstable solutions (the 'ceiling' at height $\alpha \approx +\pi/2$) are highlighted in red color. The remaining solutions consist of a 'floor' $\alpha \approx -\pi/2$ and a 'staircase' which is approximately the graph of eq.(11). The 'floor' and the 'ceiling' in Fig. 3 are only approximately horizontal due to the presence of a small but non-zero value of k_{min} through which the agent still influences the pendulum at a distance ($d > 0$).

C. Optimal Path on Graphs

In previous section, the the problem of optimally manipulating the pendulum in Fig. 1 was framed as an optimal path on the equilibrium manifold and solved specifically on the 'staircase', one of the possible branches of the equilibrium manifold, analytically defined by (11).

In real or numerical scenarios, we rarely have the luxury of an equation such as (11), locally defining a branch of the equilibrium manifold. We might just have samples of solutions, either from experiments or numerical approximations, and there might be no indication of which branch they belong to (or prior knowledge of the number of branches). In fact, the plots in Fig. 3 resemble this situation: all we have are *disconnected solutions*, each representing an equilibrium point in and open $\mathcal{Z} \times \mathcal{U} \in \mathbb{R}^{N \times K}$. We shall here only focus on the stable equilibria: numerically, we can always test the Hessian $\det(\nabla_{\boldsymbol{zz}} W)$ while, experimentally, we will not be able to even witness unstable equilibria (just like we never witness a tossed coin landing and standing on its edge).

To capture the topology of the problem, we propose working on *graphs*. Referring to textbooks such as [7] for details, here we simply recall the following basic definition: an undirected graph is a pair $\mathcal{G} = (\mathcal{V}, \mathcal{E})$ where $\mathcal{V}$ is a set of vertices and $\mathcal{E}$ is a set of edges, where each element $e_{ij} \in \mathcal{E}$ consists of an (unordered) pair of vertices $v_i, v_j \in \mathcal{V}$. Two vertices are connected (i.e. 'neighbors' in some sense, to be specified) if there is an edge connecting them.

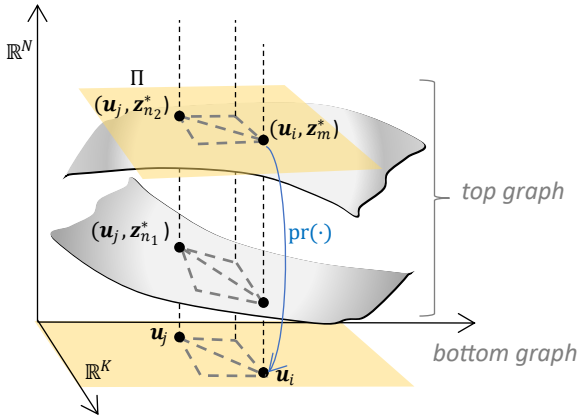

Fig. 4. Construction of connectivity in the top-graph' (in full configuration space $\mathbb{R}^N \times \mathbb{R}^K$) given the connectivity in the 'bottom-graph' (in control space $\mathbb{R}^K$). The sketch depicts (parts of) two branches of the EM lying 'above' the control point $\boldsymbol{u}_j \in \mathbb{R}^K$ and relative to different multiplicities ($\boldsymbol{z}_{n_1} \neq \boldsymbol{z}_{n_2}$). Not shown in this figure is the fact that these two branches might actually reconnect above some set of *critical* points $\boldsymbol{u}_c \in \mathbb{R}^K$ but, for this to happen, the Hessian $\nabla^2_{\boldsymbol{zz}} W$ must be rank-deficient when evaluated at $(\boldsymbol{z}_c, \boldsymbol{u}_c)$ and condition (4) no longer holds.

With reference to Fig. 4, given the control nature of the problem, we assume that an initial graph, referred to as 'bottom graph' $\mathcal{G}_{bot}$, is available. In practice, this corresponds to having an array (often a regular grid) of S control inputs $\{\boldsymbol{u}_s \in \mathcal{U}\}_{s=1}^S$. These sampling locations constitute the set of vertices for the given bottom graph $\mathcal{G}_{bot}$. With reference to the pendulum problem in Fig. 1, the inputs $\boldsymbol{u}_s$ are taken to be a regular grid of a region of the workspace and two vertices are considered connected if they are neighbors in this regular grid. Figure 4 depicts two vertices $\boldsymbol{u}_i, \boldsymbol{u}_j \in \mathcal{U}$ of the bottom graph and an edge (diagonal, dashed line) connecting them. The other edges (forming parallelogram) represent connections to other neighbors and this connectivity pattern is used to tile up the whole grid.

The objective is to construct a 'top graph' $\mathcal{G}_{top}$ given the bottom one $\mathcal{G}_{bot}$. More specifically, given isolated solutions which constitute the vertices of $\mathcal{G}_{top}$ and which naturally project to vertices on $\mathcal{G}_{bot}$, the objective is to re-construct the connectivity on $\mathcal{G}_{top}$ based on the connectivity on $\mathcal{G}_{bot}$.

To each vertex $\boldsymbol{u}_i$ on $\mathcal{G}_{bot}$ there correspond possibly multiple vertices, denoted as $(\boldsymbol{z}^*_m, \boldsymbol{u}_i)$, in $\mathcal{G}_{top}$, where $m = 1, 2, \ldots,$ is the multiplicity of solutions of (3). Since each solution $\boldsymbol{z}^*_m$ is found only after the control input $\boldsymbol{u}_i$ is specified, there exists a **natural projection**

$$\text{pr} : (\boldsymbol{z}^*_m, \boldsymbol{u}_i) \mapsto \boldsymbol{u}_i \tag{18}$$

Problem Statement: Given a solution (vertex) $(\boldsymbol{z}^*_m, \boldsymbol{u}_i)$ on the top graph and control $\boldsymbol{u}_j$ connected to $\boldsymbol{u}_i$ on the bottom graph, we would like to establish which of the solutions $(\boldsymbol{z}^*_n, \boldsymbol{u}_j)$ projecting to $\boldsymbol{u}_j$ should be connected to $(\boldsymbol{z}^*_m, \boldsymbol{u}_i)$. In other words, which of the solutions $(\boldsymbol{z}^*_n, \boldsymbol{u}_j)$ lies on the same branch as $(\boldsymbol{z}^*_m, \boldsymbol{u}_i)$.

Assuming a relatively dense grid, the idea is to numerically approximate a branch with a tangent space at $(\boldsymbol{z}^*_m, \boldsymbol{u}_i)$. Therefore, of all possible solutions $\boldsymbol{z}^*_n$ projecting down on the same $\boldsymbol{u}_j$, we should consider the one for which $\boldsymbol{z}^*_n$ is 'closest' to $\boldsymbol{z}^*_m + \delta \boldsymbol{z}_{j,i,m}$) where, from eq.(6),

$$\delta \boldsymbol{z}_{j,i,m} = -(\nabla^2_{\boldsymbol{zz}} W|_{*mi})^{-1} \nabla^2_{\boldsymbol{uz}} W|_{*mi} (\boldsymbol{u}_j - \boldsymbol{u}_i) \tag{19}$$

where the notation $|_{*mi}$ denotes that the gradients are evaluated at $(\boldsymbol{z}^*_m, \boldsymbol{u}_i)$.

This is sketched in Fig. 4), where the plane Π is tangent at $(\boldsymbol{z}^*_n, \boldsymbol{u}_j)$ to the m-th branch, according to eq.(6).

Remark [fiber-wise distance]: The reasoning above made use of the concept of 'closeness' between $\boldsymbol{z}^*_n$ and $\boldsymbol{z}^*_m + \delta \boldsymbol{z}$. This distance is evaluated on the 'fiber' above $\boldsymbol{u}_j$ and this distance is inherent to the mechanical configuration of the space $\mathcal{Z} \in \mathbb{R}^N$. We assume a fiber-wise distance, perhaps multiple ones, can always for a given problem at hand. In the specific case of the pendulum, it simply refers to difference in orientation α between two configurations and such a difference is evaluated *modulo* 2π

Once a connectivity is built on $\mathcal{G}_{top}$, each edge can be assigned a **non-negative weight**: if two vertices $(\boldsymbol{z}^*_n, \boldsymbol{u}_j)$ and $(\boldsymbol{z}^*_m, \boldsymbol{u}_i)$ of the top graph $\mathcal{G}_{top}$ are connected, a non-negative weight $w_{j,i,m}$ is defined as the squared-Hessian:

$$w_{j,i,m} := (\boldsymbol{u}_j - \boldsymbol{u}_i)^T \boldsymbol{G}|^2_{*mi} (\boldsymbol{u}_j - \boldsymbol{u}_i) \tag{20}$$

where $\boldsymbol{G}|_{*mi}$ is the Hessian defined in (8) and evaluated at $(\boldsymbol{z}^*_m, \boldsymbol{u}_i)$.

Standard search algorithms are available for finding optimal paths on graphs given non-negative weight connectivity. Fig. 5 shows a graph $\mathcal{G}_{top}$ obtained from numerical solutions following the procedure described above. An optimal path is highlighted connecting two points, chosen to be on different branches. One noteworthy aspect is that the the only way to go up on the 'staircase' (i.e. reversing the pendulum) is to pass through the intersections between 'floor' and 'staircase'. In this sense, the algorithm is able to navigate a multivalued map, finding passageways in-between branches.

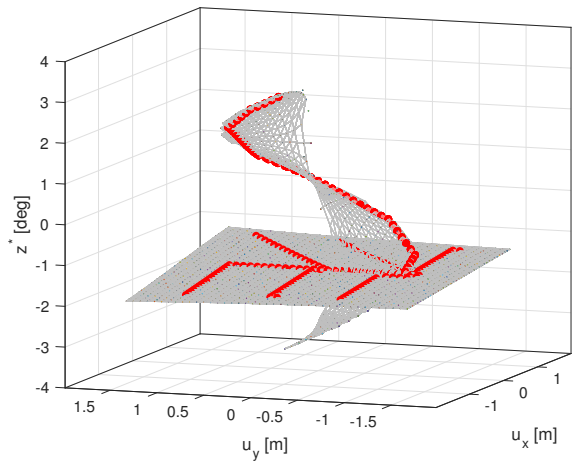

Fig. 5. Minimum paths over the top-graph $\mathcal{G}_{top}$ connecting several (arbitrary) initial points to the same final point, which lies on a different branch. All paths go through the intersection between the two branches, corresponding to the the fact that the agent has to make physical contact with the pendulum, in order to invert it.

We believe that this might lead to a topological description of the manipulation tasks.

ACKNOWLEDGMENT

This research is supported[9] by the National Research Foundation, Singapore, under the NRF Medium Sized Centre scheme (CARTIN).

REFERENCES

[1] Arnold, V. I. (1989). Mathematical methods of classical mechanics (Vol. 60). Springer Science and Business Media.
[2] Bazant, ZP and Cedolin, L (2010). Stability of Structures. World Scientific.
[3] Brockett, R. W., Stokes, A. (1991). On the synthesis of compliant mechanisms. In Proceedings. 1991 IEEE International Conference on Robotics and Automation (pp. 2168-2169). IEEE Computer Society.
[4] Brogliato, B. (1999). Nonsmooth mechanics (Vol. 3). London: Springer-Verlag.
[5] Bullo, F. and Lewis, A. D. (2005). Geometric control of mechanical systems: modeling, analysis, and design for simple mechanical control systems (Vol. 49). Springer.
[6] Campolo, D., Cardin, F. (2023). A Basic Geometric Framework for Quasi-Static Mechanical Manipulation. arXiv preprint arXiv:2307.10489.
[7] Edelsbrunner, H., Harer, J. L. (2022). Computational topology: an introduction. American Mathematical Society.
[8] Gilmore, R. (1981) Catastrophe Theory for Scientists and Engineers. Wiley, New York.
[9] Jaklic, A., Leonardis, A., Solina, F., Solina, F. (2000). Segmentation and recovery of superquadrics (Vol. 20). Springer Science & Business Media.
[10] Kana, S., Tee, K. P., Campolo, D. (2021). Human–robot co-manipulation during surface tooling: A general framework based on impedance control, haptic rendering and discrete geometry. Robotics and Computer-Integrated Manufacturing, 67, 102033.
[11] Kurtz, V., Lin, H. (2022). Contact-Implicit Trajectory Optimization with Hydroelastic Contact and iLQR. arXiv preprint arXiv:2202.13986.
[12] LaValle, S. M. (2006). Planning algorithms. Cambridge university press.

[9]Any opinions, findings and conclusions or recommendations expressed in this material are those of the author(s) and do not reflect the views of National Research Foundation, Singapore.

Algorithm 1: Top-Graph construction

Input:
- $\mathcal{G}_{bot} = (\mathcal{V}_{bot}, \mathcal{E}_{bot})$ where $\mathcal{V}_{bot} = \{\boldsymbol{u}_1, \boldsymbol{u}_2, \ldots, \boldsymbol{u}_S\}$;
- heuristic threshold d_{min};

$\mathcal{V}_{top} \leftarrow \emptyset$;
for $i = 1 \ldots |\mathcal{V}_{bot}|$ **do**
  Determine $\{\boldsymbol{z}^*_m\}_{m=1}^{M_i}$ such that $(\boldsymbol{z}^*_m, \boldsymbol{u}_i) \in$ EM;
  if $\nabla_{\boldsymbol{zz}} W(\boldsymbol{z}^*_m, \boldsymbol{u}_i) > 0$ **then**
    $\mathcal{V}_{top} \leftarrow \mathcal{V}_{top} \cup \{(\boldsymbol{z}^*_m, \boldsymbol{u}_i)\}_{m=1}^{M_i}$;
foreach $(m, i) : (z^*_m, \boldsymbol{u}_i) \in \mathcal{V}_{top}$ **do**
  foreach $\boldsymbol{u}_j : (\boldsymbol{u}_i, \boldsymbol{u}_j) \in \mathcal{E}_{bot}$ **do**
    if $j > i$ **then**
      foreach $(n, j) : (z^*_n, \boldsymbol{u}_j) \in \mathcal{V}_{top}$ **do**
        $\delta \boldsymbol{z}_{j,i,m} \leftarrow -\nabla^2_{\boldsymbol{zz}} W|^{-1}_{*mi} \nabla^2_{\boldsymbol{uz}} W|_{*mi} (\boldsymbol{u}_j - \boldsymbol{u}_i)$;
        if $\|z^*_n - z^*_m - \delta \boldsymbol{z}_{j,i,m}\|_{\mathbb{R}^N} \leq d_{min}$ **then**
          $w_{j,i,m} \leftarrow (\boldsymbol{u}_j - \boldsymbol{u}_i)^T \boldsymbol{G}|^2_{*mi} (\boldsymbol{u}_j - \boldsymbol{u}_i)$;
          if $w_{j,i,m} > 0$ **then**
            $\mathcal{E}_{top} \leftarrow \mathcal{E}_{top} \cup \{((z^*_n, \boldsymbol{u}_j), (z^*_m, \boldsymbol{u}_i), w_{j,i,m})\}$;

Output $\mathcal{G}_{top} = (\mathcal{V}_{top}, \mathcal{E}_{top})$;

[13] Lynch, K. M., & Park, F. C. (2017). Modern robotics. Cambridge University Press.
[14] Hermansson, T., Carlson, J. S., Linn, J., Kressin, J. (2021). Quasi-static path optimization for industrial robots with dress packs. Robotics and Computer-Integrated Manufacturing, 68, 102055.
[15] Jiang, Y., Huang, Z., Yang, B., Yang, W. (2022). A review of robotic assembly strategies for the full operation procedure: Planning, execution and evaluation. Robotics and Computer-Integrated Manufacturing, 78, 102366.
[16] Loncaric, J. (1987). On statics of elastic systems and networks of rigid bodies. Maryland Univ College Park Systems Research Center.
[17] Loncaric, J. (1991). Passive realization of generalized springs. In Proceedings of the 1991 IEEE International Symposium on Intelligent Control (pp. 116-121). IEEE.
[18] Ozawa, R., Tahara, K. (2017). Grasp and dexterous manipulation of multi-fingered robotic hands: a review from a control view point. Advanced Robotics, 31(19-20), 1030-1050.
[19] Salem, A., Karayiannidis, Y. (2020). Robotic assembly of rounded parts with and without threads. IEEE Robotics and Automation Letters, 5(2), 2467-2474.
[20] Spivak, M. (2018). Calculus on manifolds: a modern approach to classical theorems of advanced calculus. CRC press.
[21] van der Schaft, A. (2021). Classical thermodynamics revisited: A systems and control perspective. IEEE Control Systems Magazine, 41(5), 32-60.
[22] Wen, K., Gosselin, C. (2021). Static Model-Based Grasping Force Control of Parallel Grasping Robots With Partial Cartesian Force Measurement. IEEE/ASME Transactions on Mechatronics, 27(2), 999-1010.
[23] Whitney, D. E. (1982). Quasi-static assembly of compliantly supported rigid parts. Journal of Dynamic Systems, Measurement, and Control, 104(1), 65-77.
[24] Yang, L., Ariffin, M. Z., Lou, B., Lv, C., Campolo, D. (2023). A Planning Framework for Robotic Insertion Tasks via Hydroelastic Contact Model. Machines, 11(7), 741.
[25] Yu, J., LaValle, S. M. (2016). Optimal multirobot path planning on graphs: Complete algorithms and effective heuristics. IEEE Transactions on Robotics, 32(5), 1163-1177.